Parametric Study of Damage Evaluation into Solid Dielectrics Due to PD Activity Using a Kinetic Model

Alireza Ganjovi
Photonics Research Institute, Institute of Science and High Technology and Environmental Sciences, Graduate University of Advanced Technology, Kerman, Iran.
Email: ganjovi@icst.ac.ir

Received: August 2013 Revised: January 2014 Accepted: March 2014

ABSTRACT
A kinetic model is used based on Particle in Cell - Monte Carlo Collision (PIC-MCC) model, for parametric study of the damage due to partial discharges (PD) activity into the surroundings dielectrics of a narrow channel encapsulated within the volume of a dielectric material. The parameters studied are applied electric field, channel dimensions and gas pressure. After employing an electric field across a dielectric material which contains a narrow channel, repeated ionization process starts in the gaseous medium of narrow channel. Charged particles, especially electrons, gain energy from the electric field across narrow channel and cause damage into dielectric surfaces of narrow channel on impact. The dependence of the electron energy distribution function (EEDF) on the applied electric field is considered. These estimations are performed based on the number of C-H bond-scissions produced by the impacting electrons of a single PD pulse. Regarding this technique, the consequent damage into the solid dielectric and the time required to increase surface conductivity, is computed. The formation of acid molecules due to interaction of PD pulse with polymer surface in presence of air and humidity causes changes in the surface conductivity of the surrounding dielectrics of the narrow channels. It is observed that the extent of damage caused by a PD is primarily determined by the total number of impacting electrons which are capable of producing bond-scission at the dielectric. Parameters that effectively cause an increase in the number of energetic electrons will increase effective damage as well as surface conductivity of surrounding dielectrics.

KEYWORDS: Partial Discharges; Dielectric Degradation; PIC-MCC Simulation; Parametric Investigation.

1. INTRODUCTION

Generally, high voltage apparatus under operating conditions are subjected to harmful effects of partial discharges' activity into surrounding dielectrics of the existing narrow channel encapsulated within the volume of a dielectric material. A PD pulse generates energetic charged particles and photons and they transfer sufficient energy to the polymer surfaces to break covalent bonds and form radicals. Usually, the polymer radicals react rapidly with oxygen [1].

The droplets of glycolic and formic acid as degradation products are identified by Hudon et al. They form initially on the surfaces of surrounding dielectrics of narrow-channel [2]. These acid molecules are much more conductive than the epoxy resin matrix, which is responsible for a rapid increase in surface conductivity [3, 4]. Moreover, when the surface conductivity is very low while spark-type PD pulses occurring, glow discharges are observed after the surface becomes more conductive [5].]. An increase in surface conductivity was initiated in polyethylene [6], not long after the PD process.[6].

The variations in discharge behavior associated with changes in the electrical characteristics of solid dielectric materials during the course of the discharge are investigated by Ishida et al. [7]. Some other authors also detected the formation of acid molecules due to interaction of discharge with polymer surfaces [8-15].

Rogers showed that 'self-extinction' of pulsating PD in a dielectric cavity can be attributed to a discharge-induced increase in the conductivity of the cavity walls [16]. The conclusions by Tanaka et al. show that the nature of discharges is influenced by physical properties of the inner-surface of a cavity [17]. They resulted that the discharge, itself, causes no change in electrical conductivity of the surface. Auckland et al. [18] observed that the charge on channel walls influenced the characteristics of breakdown in an artificial channel.

The proposed aging and life model based on electro-thermal degradation processes and space charge effects by Serra et al. [19] was useful to study the damage originating from microscopic defects such as micro-voids. They considered the degradation within a

polyethylene-based material as a bond-breaking process due to impact of hot electrons, in company with the damage accumulating with time at void-polymer interfaces.

The dependence of insulation time about applied field's failure, temperature and cavity size was studied quantitatively [20-22]. A two dimensional fluid model proposed by Novak et al. [23]. They studied the effect of charge produced by ionization on the surrounding solid insulation. They estimated the average kinetic energy of the electrons and ions about 10eV and 0.6eV, respectively.

Although the aging and life model developed by Serra et al. [19] gives an estimate of damage on cavity walls due to hot electrons, one of its major drawbacks lies in is that the electric field within the void assumed constant. Consequently the spatial distribution of charged particles (electrons) within the void is neglected.

The electron energy distribution functions (EEDF) are assumed to be space-independent. Moreover, the model is one-dimensional, so that the interaction of charged particles with the side-walls of the cavity is not considered. Novak et al. [23] used a fluid model, where transport and swarm parameters such as ionization and attachment coefficient, velocities, EDF of electrons and ions, etc must be known in advance. Therefore it becomes obvious that in terms of damage, a relatively assumption-free model capable of estimating the effects of PD pulse on channel walls in very narrow channels and surface conductivity's increasing through particle bombardment of surrounding dielectrics, are required [24-28].

. In this paper, using a two dimensional kinetic model based on PIC-MCC technique; the degradation's dependence of polymer dielectrics on some pertinent physical parameters which are characterizing the discharge within the narrow channel are investigated. For this purpose, the results of a number of simulations are presented. The simulation results are compared with existing experimental results (e. g. [1-5]) reported in the literature, wherever possible.

2. PD COMPUTATIONAL METHOD WITHIN NARROW CHANNEL

In the PIC scheme, particles are defined in a continuum position and velocity space. Field values are defined at discrete locations in space. Particle and field values are advanced sequentially in time, starting from initial conditions. The particle equations of motion are solved at every time intervals, using field values interpolated from the discrete grid to particle locations. The force on every particle is computed by interpolation of the field values from the grid position to the given particle positions. The position and velocities of each particle is next updated based on the solution of the classical equation of motion [29]. Then, particle boundary conditions are applied. For modeling collisions, the Monte Carlo collision (MCC) scheme is applied [30]. Source terms for the field equations are accumulated from the particle locations to the grid locations. The field values are then advanced by one time-step, and the time loop starts again (figure 1).

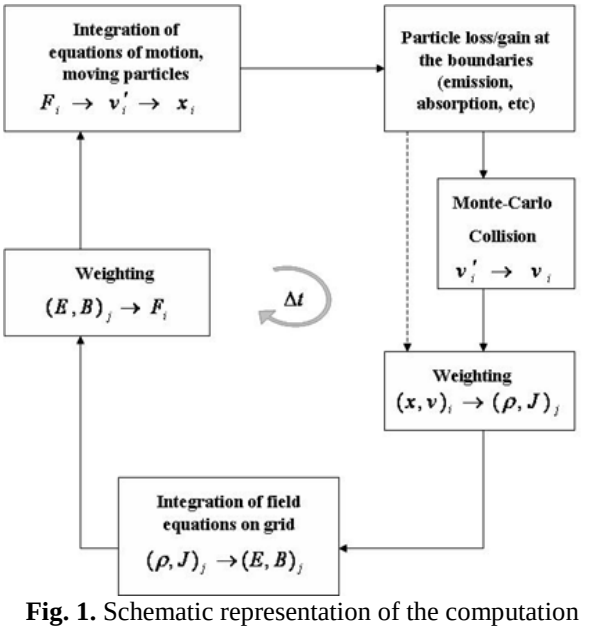

Fig. 1. Schematic representation of the computation sequence for Particle in Cell-Monte Carlo (PIC-MCC) method

In the PIC-MCC scheme, each super-particle, representative of one or a much larger number of real particles, is designated in continuum space by its position and velocity. Initially, a Maxwellian distribution is assumed for electrons and ions. Further, the particles are uniformly distributed in the gap space. Particle boundary conditions such as absorption and emission are used to account for the relation between the discharge current in the gap and the current in the external circuit. When an electron or ion passes from the discharge into an end wall, it adds to the wall charge and is deleted from the list of active particles [27]. Additionally, secondary emissions occur when a charged particle impacts a surface (metallic or dielectric) causing ejection of electrons from the surface.

In the current work, the gas within the cavity is assumed to be air at atmospheric pressure. Therefore, photo-emission at the cathode is likely to be the dominant secondary emission process, rather than electron emission from cathode or anode due to ion or electron bombardment. However, all of the above processes have been accounted for in the model. After emission of a new electron, its energy is also assigned from an assumed Maxwell-Boltzmann distribution. The

interaction of charged particles with neutral atoms and molecules, and other collisional processes are included by using a Monte Carlo Collision technique [31]. Three main charged particle species, viz. electrons, positive ions and negative ions have been considered. The major electron-neutral molecule impact reactions included are (i) elastic, (ii) excitation, (iii) ionization (including all important ionization reactions) and (iv) electron attachment. Related cross sectional values are extracted from experimental data available in the literature [28]. Integral cross section values for electron interaction in dry air have been determined from its molecular constituents by assuming a target composition of 78.09%N_2 and 21.19%O_2 [32]. Only elastic and charge transfer collisions between ions and neutrals are considered. Because ion-molecule cross sections are not readily available, a constant cross section ($10^{-20}m^2$) has been assumed based on a hard-sphere collision model [33].

A significant contribution of this work is that the discharge within the cavity is simulated in conjunction with an external circuit comprising of a voltage source, and a blocking capacitor that stops the flow of any average current. The coupling between the charge flow within the micro-cavity and the external current is obtained via the parallel-plane electrodes, which may be metallic or dielectric, depending on the location of the discharge site.

The potentials and fields are obtained using Poisson's equation:

$$\nabla \cdot \varepsilon_0 \nabla \Phi(x,t) = \rho(x,t) \tag{1}$$

The potential (Φ) can be separated as follows [31, 34, 35]:

$$\Phi = \Phi_P + \sum_{Boundaries} \Phi_L \tag{2}$$

where Φ_P and Φ_L represent the Poisson and Laplacian parts of electrical potential (Φ).

Therefore, the field may be described by the combination of the following equations:

$$\nabla \cdot \varepsilon_0 \nabla \Phi_P = -\rho \tag{3}$$

$$\nabla \cdot \varepsilon_0 \nabla \Phi_{Li} = 0 \tag{4}$$

The boundary condition for equation (3) is Φ=0 on all boundaries as the Poisson field is solely due to charge in the medium. For each boundary with a Dirichlet condition, equation (4) is solved for Φ_i=0 on the equipotential surface, and Φ=0 elsewhere which gives us Φ_{Li} (the potential due to the i^{th} Laplacian field). Φ_L is obtained by the superposition of all the Laplacian fields. Neumann boundary conditions are included through Φ_P=0. This method neglects charges induced by a driven electrode on other boundaries which are connected to an external circuit. It is also possible to solve the field Poisson equation with boundaries and circuits [31, 29, 36].

In this work, identical cavities, as might occur at discharge sites, with two different electrode configurations have thus been considered. These are the two generic cases described below. The model is two-dimensional with Neumann boundary conditions on the side-walls. Dirichlet boundary conditions (potential drop specified) are assumed on the electrodes.

A narrow channel bounded by dielectrics on both sides is depicted in Figure 2(a).

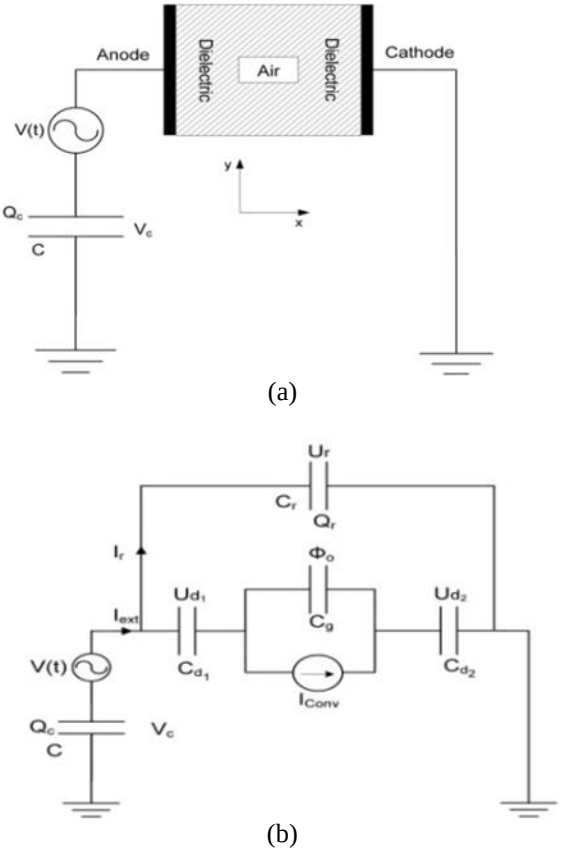

Fig. 2. (a) The geometry of two dimensional dielectric-dielectric narrow channel; the external circuit consists of a voltage source and a blocking capacitor which stops the flow of average current, (b) the corresponding equivalent circuit

The equivalent circuit of this configuration is shown in Figure 2(b), where C_g, C_{d1}, C_{d2} and C_r represent the equivalent capacitances of the gap, the dielectric layers and materials parallel to the micro-channel, respectively. The discharge current may be represented by I_{conv}. Using KCL, it is possible to obtain the following relations [25]:

$$C_d \frac{dU_d}{dt} = I_{ext} - I_r \tag{5}$$

$$A\frac{d\sigma_s}{dt} = I_{ext} - I_r + AJ_{conv} \quad (6)$$

$$V_c = V(t) - 2U_d - \phi_0 \quad (7)$$

$$U_r = 2U_d + \phi_0 \quad (8)$$

where I_{ext} and σ_T are the total external current and charge on the dielectric surface. I_r is the leakage current flowing in the bulk of dielectric material parallel to the narrow channel. By combining the above equations, equation (27) in ref. [25] may be rewritten as follows:

$$\varphi_0^t = (\sigma_{s_T}^{t-1} + \frac{1}{A}(\alpha CV(t) - \alpha Q_c^{t-1} + \alpha Q_r^{t-1} - 2\alpha(C + C_r)U_d^{t-1} + Q_{Conv}^t) + \frac{\Delta x}{2}\sum_{j=0}^{j=N}\rho_{0j} + \frac{\varepsilon}{\Delta x}\sum_{j=0}^{j=N}\varphi_{1j}^t)(\frac{\varepsilon}{\Delta x}N + \alpha(C + C_r)/A)^{-1} \quad (9)$$

where $\alpha=(1+2(C+C_r)/C_d)^{-1}$. Σ_T, A, C, V(t), Q_c, Q_r, Q_{conv}, ρ, φ_{ij} and N_j are respectively the total surface charge density on the electrodes at a given time 't', cross sectional area of electrode, capacitance of blocking capacitor, driving voltage, charge in the external circuit, charge in the bulk of dielectric material parallel to the narrow channel, charge convection due to discharge, space charge density, the electric potential at each grid point and the number of grid divisions along the y-axis. The derivation of equation (5) is presented in appendix 1.

3. DAMAGE AND CHANGE'S COMPUTATION IN SURFACE CONDUCTIVITY

In this section, the methodology adopted for computation of damage is described. Electrons produced within a narrow channel during a PD pulse, are accelerated by the applied field and reach the dielectric electrode with high energies. Additionally, during transition, they may also strike the dielectric side-walls of the narrow channel. The trajectory of each electron participating in the discharge is followed until it strikes a dielectric surface (wall or anode). The energy distribution functions (EEDF) of the electrons at the dielectric anode and the dielectric side walls, are computed. The dielectric is assumed to be epoxy resin, which has a preponderance of C-H and C-C bonds. The impact of the electrons on the dielectric may cause chemical degradation of the material. In this work, the damage is assessed solely in terms of the amount of polymer that undergoes C-H bond scission through electron impact. The dissociative electron attachment (DEA) or ionization of C-H bonds requires approximately 8eV [19]. The damage due to each electron impact is computed in the following manner. Table 1 shows the electrons divided into a number of groups. Of the groups outlined in Table 1, the first group (g_1) contains electrons with energy less than 8eV (ε< 8eV). These are cold electrons, and are considered to be irrelevant from the point of damage accumulation, as they are unable to produce irreversible degradation [19]. Electrons belonging to the remaining groups have energies beyond 8eV, and are capable of causing bond-scission. In every scattering event, an electron loses approximately 8eV, and shares the remaining energy equally with a secondary electron produced by impact ionization. Each electron is allowed to go through several scattering processes until its energy falls below 8eV. Thus, all high energy electrons ultimately get cool to energy values smaller than 8eV [19-22, 37].

Table 1. The number of C-H bonds scissions due to one electron (N_k) for different electron energy groups

Group	Electron energy domain	N_k
g_1	ε<8eV	0
g_2	8eV≤ε<24eV	1
g_3	24eV≤ε<56eV	3
g_4	56eV≤ε<120eV	7
g_5	120eV≤ε<248eV	15
g_6	248eV≤ε<504eV	31

Electrons belonging to group g_2, possess energies between 8eV and 24eV. This energy is sufficient to cause only one C-H bond-break, as the excess energy when shared between a primary and a secondary, produces cold electrons. The subsequent groups are based on the number of C-H bond-scissions that caused by the respective groups' electrons before they thermalize. The thermalization process is very fast, i.e. of PD pulse duration (<50ps) [19, 20]. The number of C-H bond-scissions due to any electron in group g_k, may thus be expressed as ($N_k=2^{k-1}-1$). The number of C-H bonds which can be broken by one PD pulse (n_{CH}) is calculated as the sum of bond-breaks by all electrons belonging to groups g_2 to g_6 (normally electrons with higher energies than those pertaining to g_6 are not produced in a single PD event), as shown below:

$$n_{CH} = \sum_{k=2}^{6}(2^{k-1} - 1)N_{gk} \quad (10)$$

where N_{gk} is the number of electrons in the respective group (g_2 to g_6).

Diglycidyl ether of bisphenol-A (DGEBA) is a typical commercial epoxy resin and is chosen, in this work, as the base material to illustrate the mechanism of damage computation. Figure 3 shows the molecular structure of DGEBA.

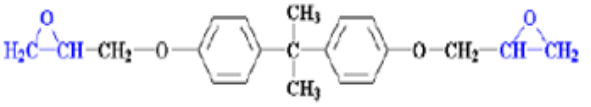

Fig. 3. Molecular formulae of DGEBA monomer

Thus, each DGEBA monomer has 24 C-H bonds. The radius of a DGEBA monomer is approximately R(≈13.28A^0) [38], and its cross-sectional area is approximately $A_{DGEBA}=5.546\times10^{-18}m^2$. The cross sectional area of the dielectric anode is $A_{anode}=L_y\times L_z$ and the area of each side wall is $A_{side\text{-}walls}=L_x\times L_z$. The number of DGEBA monomers on the surface of the dielectric anode and cathode is thus approximately $(N_{DGEBA})_{anode} = (N_{DGEBA})_{cathode} = A_{anode}/A_{DGEBA}$, and that on the surface of side wall is $(N_{DGEBA})_{side\text{-}walls} = A_{side\text{-}walls}/A_{DGEBA}$. The areas degraded from the dielectric anode and side-walls due to one PD pulse are estimated as follows:

$$\delta A_{anode} = \left(\frac{n_{CH}}{24\times N_{DGEBA}}\right)_{anode} A_{anode}$$
$$\delta A_{side-wall} = \left(\frac{n_{CH}}{24\times N_{DGEBA}}\right)_{side-wall} A_{side-wall} \quad (11)$$

Chemical analysis of the deteriorated region in a micro-channel using microanalysis [39] showed that as a result of the intense spark discharge activity, complex chemical reactions take place between the plasma and the polymer surface. Energetic electrons (> 4.3eV) from the discharge transfer sufficient energy to the polymer surface to break covalent bonds (C-H bonds), thus giving rise to radical formation from epoxide groups in DGEBA monomer. It is commonly assumed in the literature [1-5, 10-14, 40] that surface oxidation during discharge treatment is via a free radical process which is presented in figure 4.

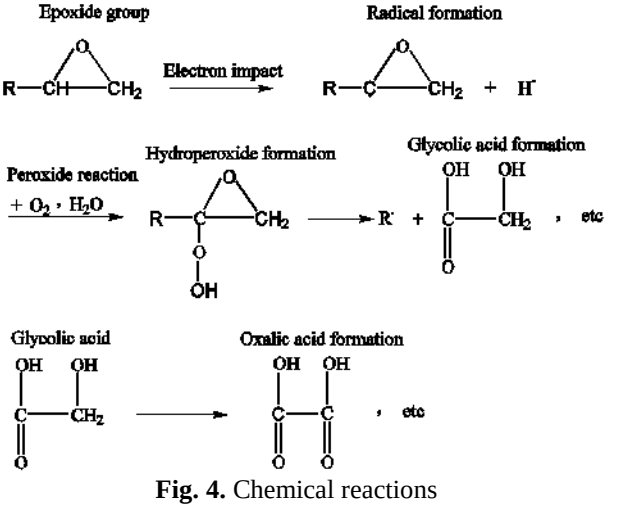

Fig. 4. Chemical reactions

The water may either be present as trapped moisture in the epoxy matrix, or it may originate as one of the degradation by-products. The first few steps probably occur during the large pulse discharge (spark-type) regime [1]. The formation of the oxalic acid crystals, constitutes the final step of the reaction sequence, and is predominantly manifest during the pseudo-glow and glow discharge regimes. The results of Hudon et al for evaluation of surface conductivity with time suggest that droplets (formed in presence of spark discharges) have a more pronounced effect on surface conductivity than the crystals formed under glow discharge conditions [1-5]. Morshuis et al. showed that if one of the constituents H, C or O was absent, no droplet appeared [6, 41].

The breaking of C-H bonds due to electrons in DGEBA monomer requires at least 4.3eV. Based on chemical reactions presented in figure 3, it is assumed that each epoxide ring is responsible for formation of only one acid molecule. So, every DGEBA monomer containing two epoxide rings would produce only two acid molecules (figure 3). We further assume for the sake of convenience, that the cross section of each acid molecule is equal to that of one epoxide ring. The process of C-H bond breaking in DGEBA monomer is assumed to be probabilistic event. The probability of a C-H bond break is calculated as:

$$P = 2(\pi r^2/\pi R^2)/3, \quad (12)$$

where r(≈2A^0) and R are the radius of epoxide ring and DGEBA monomer, the coefficient '3' in the denominator owes its existence to three C-H bond in every epoxide ring. The number of acid molecules (N_a) which can be formed due to one PD pulse is obtained as $(N_a)_{anode} = P\times(N_{CH})_{anode}$ and $(N_a)_{side\text{-}walls} = P\times(N_{CH})_{side\text{-}walls}$ on dielectric anode and side-walls, respectively. So, the number of PD pulses (N_p) which are required to convert all the existing epoxide rings to acid molecules may be obtained as follows:

$$(N_p)_{anode} = 2\times(N_{DGEBA})_{anode}/(N_a)_{anode}$$
$$(N_p)_{side-walls} = 2\times(N_{DGEBA})_{side\text{-}wall}/(N_a)_{side-walls} \quad (13)$$

The coefficient "2" is due to presence of two epoxide rings in each DGEBA monomer. Again, the number of cycles required to convert all epoxide groups to acid is as follows:

$$(N_{cycle})_{anode} = (N_p)_{anode}/N_{PDC}$$
$$(N_{cycle})_{side-walls} = (N_p)_{side-walls}/N_{PDC}, \quad (14)$$

where N_{PDC} indicates the number of PD pulses per cycle [42-45].

Hence, the time required to convert all epoxide rings to acid molecules at a supply frequency of 50Hz (T=20ms) may be calculated as follows:

$$(t_c)_{anode} = T \times (N_{cycle})_{anode}$$
$$(t_c)_{side-walls} = T \times (N_{cycle})_{side-walls} \quad (15)$$

where t_c is the required time to convert all epoxide rings to acid molecules.

4. SIMULATION RESULTS

In this paper, the simulations are performed with the chosen parameters presented in table 2. It may be noted that a channel with a significantly large length / width ratio is chosen.

Table 2. Simulation data

Property	Symbol	Value
Length of Narrow channel	L_x	20 µm
Width of Narrow Channel	L_y	1 µm
Depth of Narrow Channel	L_z	1 µm
Dielectric thickness	L_d	20 µm
Background gas pressure	P_g	101325 Pa
Background gas temperature	T_g	0.026 eV
External capacitor	C	40 pF
Initial number of charged	n_f	10
Photo-emission coefficient	λ_{ph}	5×10^{-5}
Ion-induced emission	λ_i	1.5×10^{-3}
Dielectric constant of air	ε_0	8.85×10^{-12}

Parameters used to characterize the damage of the surrounding dielectrics due to the discharge, as discussed in the previous section are presented in table 3. The kinetic energy of the electrons (KE) impinging on the dielectric anode is higher than side-walls. So, it causes a higher fractional area (δA/A) of the dielectric anode to be degraded compared to the side-walls. . The conversion time of the epoxide rings to acid molecules (t_c) for dielectric anode is much lower than (two orders) side-walls. This would indicate that given the occurrence of a sufficient number of spark-type PD pulses, the discharge is likely to change from pulse-type to glow, rather than discharge extinction that would have been encouraged by a high increase in surface conductivity of the side-walls. This is in qualitative agreement with the experimental results reported by Hudon et al. [3, 4]. Hudon et al. [1-5] observed that for a specimen stressed for very long times (e. g. 900 h), the increase in surface conductivity observed by at least 7 orders of magnitude from an initial value ($\kappa\approx10^{-16}$S) occurred mainly during the first 3 hours of exposure. A change in the behavior of the PD's occurred between 180 to 320 h. It must be noted that the transition times from spark-type to glow discharge mentioned by Hudon et al. [3-5], are considerably larger than the times reported in current simulation (table 3). The reasons could be several: (1) The much larger cross sectional area of the dielectric anode perpendicular to applied electric field (A= $\pi\times0.05^2$ m^2) [3, 4] as compared to A=10^{-6} m×10^{-6} m in our simulations. (2) In this work we assume all epoxide rings readily convert to acid molecules (liquid phase). In fact, when sufficient quantity of acid droplets is produced, the liquid would take time to spread over the dielectric anode surface and make it conductive.

Table 3. Typical simulation results (For electric field of E=40 kV/mm)

	Dielectric Anode	Dielectric Side-walls
KE (eV)	12.90	11.40
δA/A	6.969×10^{-5}	6.964×10^{-6}
t_c(s)	5.32	1826
x^D/L_x	-	0.1045

The studied parameters are as following: applied electric field, narrow channel dimensions, gas pressure inside channel.

The scatter plots in phase space for velocities in x-direction i. e. (V_x, x, y) for electrons, and positive ions inside the micro-channel are shown in figures 5 and 6 at particular instants of time. As shown here, drift velocity of electrons is much greater than that of ions (3 orders of magnitude higher) and quickly traverse the micro-channel length. All charged particles are distributed about the center-line y=50µm. Most of charged particles are created very close to the anode. The number of ions near the anode increases through ionization with passage of time. The positive ions slowly drift towards the cathode, till at about 600 ps the entire gap distance is almost evenly populated. From this time onwards, ions gradually leave the channel, thus depleting the ion density in the gap. This is similar to the evolution of the electrons within the gap, as seen in figure 6, except that electrons move faster and need travel only a small distance between the ionization region and the anode. As is clear from figure 6, ion velocities increase as they reach near the cathode, accelerated by the electric field. Generally, owing to high electric field strength along micro-channels, attachment process is weak and the production of negative ions is low

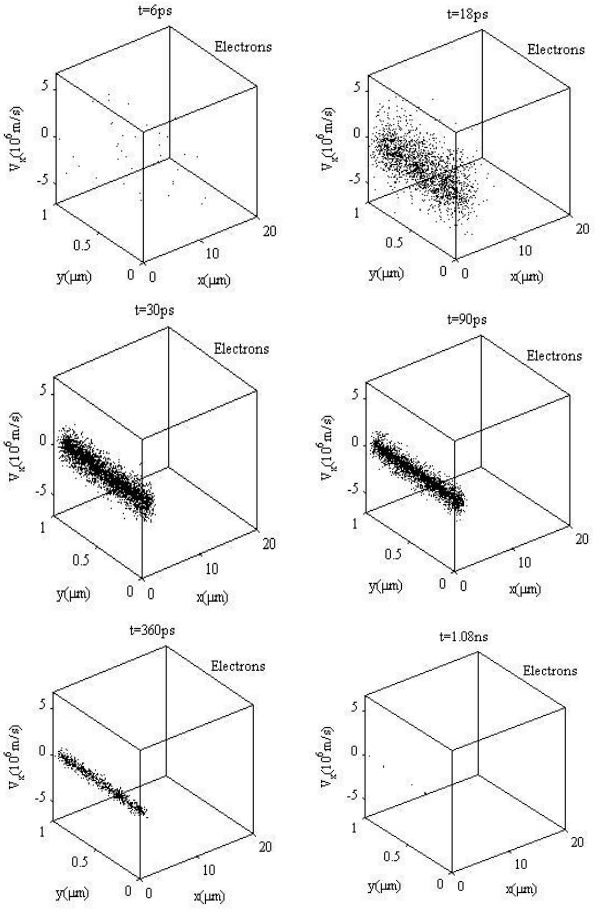

Fig. 5. Scatter plot of electrons in the phase-space (V_x, x, y) inside the micro-channel at particular instants of time

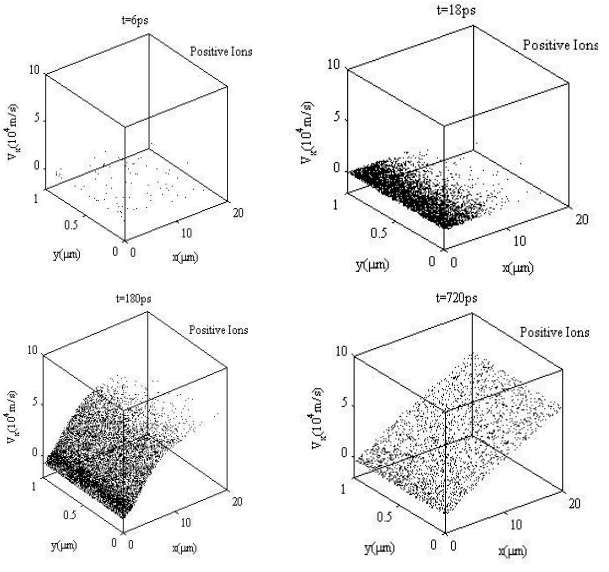

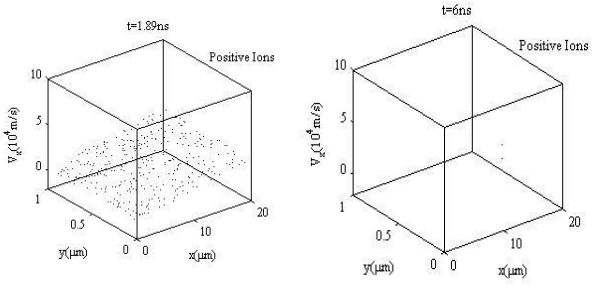

Fig. 6. Scatter plot of positive ions in the phase-space (V_x, x, y) inside the micro-channel at particular instants of time

4.1. Applied Electric Field

Simulations are performed with the operating parameters specified in table 2. The dielectric material surrounding the channel is assumed to be DGEBA as before. We confine ourselves to the issue of C-H bond scission due to electron impact.

Table 4 shows the group composition of electrons (N_{gk}) impacting the dielectric anode at different applied electric fields With higher electric fields, the total number of electrons reaching the dielectric anode is higher due to greater ionization. This matches the observation by Serra et al. [19] that the number of electrons generated inside a cavity increases with applied electric field. Also, understandably, increase in applied electric field results in larger proportion of hot electrons being produced.

Table .4. Group composition of electrons (N_{gk}) impacting the dielectric anode at different applied electric fields.

E(kV/mm)	N_{g1}	N_{g2}	N_{g3}	N_{g4}	N_{g5}
8	18	11	4	0	0
10	72	49	4	0	0
20	150	145	71	2	0
30	1610	792	344	63	1
40	2584	1083	596	171	9
50	5317	1441	932	361	36

Figures 7(a) and 7(b) show the Energy Distribution Functions (EEDF) of the electrons reaching the dielectric anode and side-walls. Increase in applied field is accompanied by a decrease in the proportion of cold electrons (< 10 eV. Thus, the average kinetic energy of electrons (electron temperature) at the dielectric anode is seen in figure 7(c) to increase with field; the electrons acquire higher energies as they are accelerated in the stronger electric field within the narrow channel.

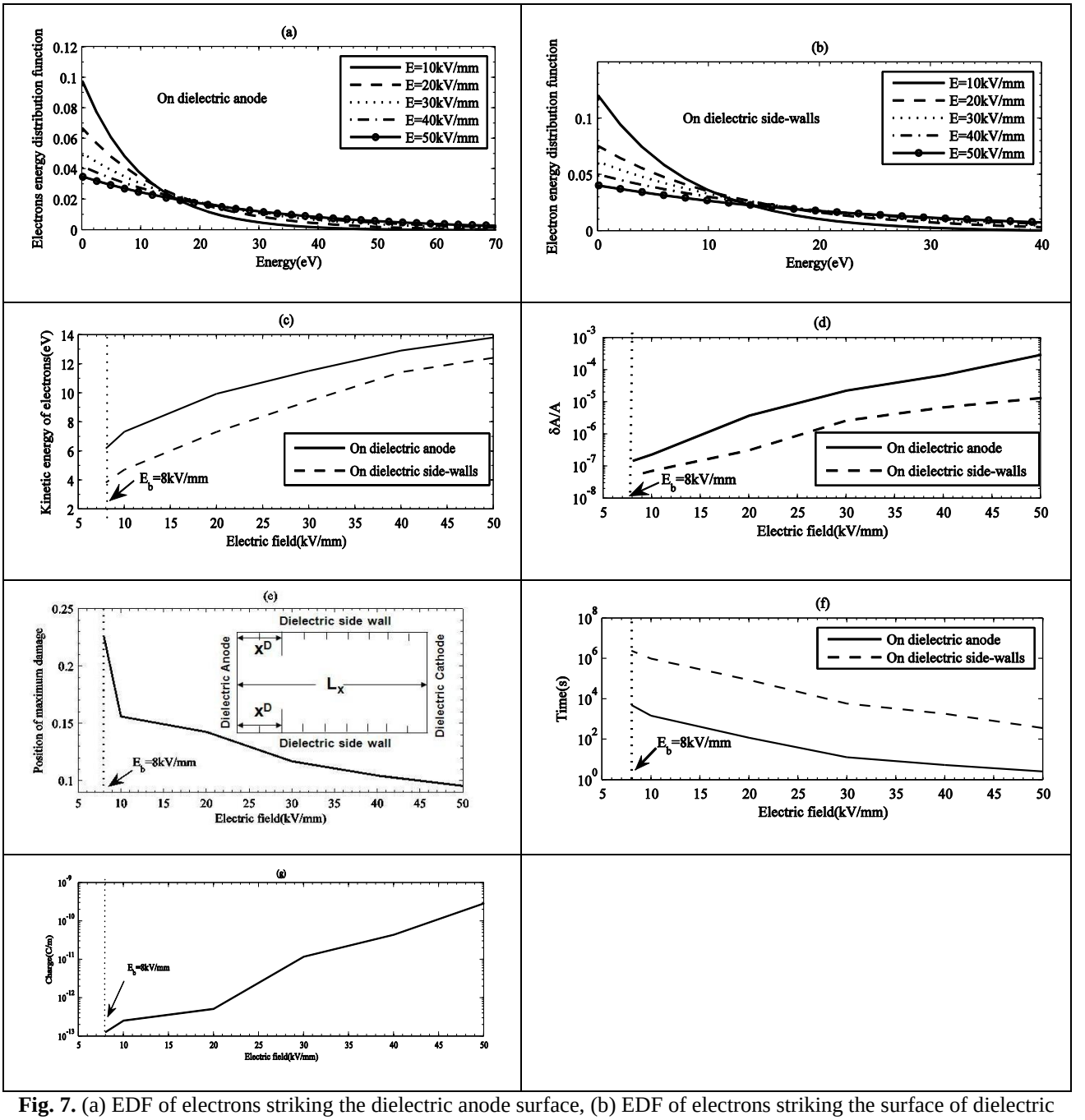

Fig. 7. (a) EDF of electrons striking the dielectric anode surface, (b) EDF of electrons striking the surface of dielectric side walls, (c) Average kinetic energy of electrons striking the dielectric anode and side walls, (d) Variation of fractional area damaged (δA/A) during one PD pulse on dielectric anode and side-walls as a function of electric field across narrow channel, (e) Distance (normalized) from dielectric anode of region of maximum damage (x^D/L_x) on dielectric side walls, (f) The time of conversion of entire of epoxide rings to acid molecules (t_c) on dielectric anode and side-walls as a function of electric field across narrow channel, (g) Charge trapped to narrow channel side-walls during one single PD pulse as a function of electric field narrow channel

The combined effect of increased number of impacting electrons, and higher average energy of impacts, contribute to a higher number of C-H bond-scissions; a greater percentage of the dielectric anode surface is thereby degraded. As shown in figure 7(d), the effect of field on the extent of damage on the dielectric side-walls of the channel is similar to that on the dielectric anode. Kinetic energy, and therefore, degradation at the side walls increases at a steeper rate than at the dielectric anode, as a comparison of figures 7I and 7(d)

shows. A simple parametric fit on fractional area damaged (δA/A) for dielectric anode and side walls with electric field indicates a higher proportionality at the dielectric anode as given below:

$$\left(\frac{\delta A}{A}\right)_{\text{anode}} \propto (E)^{8.6} \qquad \left(\frac{\delta A}{A}\right)_{\text{side-wall}} \propto (E)^{6.75} \tag{16}$$

where $(\delta A/A)_{anode}$ and $(\delta A/A)_{side\text{-}walls}$ are respectively the fractional damaged area on dielectric anode and side-walls of narrow channel. The quantity (δA/A) during one PD pulse is somewhat comparable to the "damage growth rate" of dielectric-void interface obtained by Montanari et al. [19-22] in his aging model. Their estimation of the damage growth rate is based on the amount of energy dissipated in the insulating material surrounding a cavity, and obtained as the ratio of the thickness of the slab damaged (D_{dis}) to the total time (t_{dis}) required to dissociate at least half of the CH bonds inside this dielectric slab.

Interestingly, dielectric side-walls are not uniformly impacted by the damage-inducing electrons. The average distance at which the dielectric side-walls are struck is shown in Figure 7(e). As may be seen, regions very close to the anode (near 25% of the total channel length at lower electric fields of 8 kV/mm) are most damaged. The damaged region takes place closer to the anode at higher applied electric fields for example, around 10% for electric field with value of 50 kV/mm.

Figure 7(f) shows the effect of applied electric field on the time taken to convert all the epoxide rings on dielectric anode and side walls to acid molecules (t_c). The larger number of electrons and increased average kinetic energy of the electrons reaching the surrounding dielectrics (figure 7c), contribute to a reduction in the time for conversion of the epoxide rings on dielectric anode and side walls to acid molecules (t_c) in both cases. The conversion time varies sharply with field, e.g. from 80 min to 2.53 s for dielectric anode, as the field increases from 8 kV/mm to 50 kV/mm. This would essentially mean an increased surface conductivity at higher electric fields, given the same time of exposure to discharge.

Two types of discharge pulse forms, a spark-type and smaller Townsend, have been reported [1-5] to occur within micro-channels. Kaminaga et al. reported that a free radical is generated in the initial phase of degradation of Polyethylene in high electric fields [47]. These free radicals are expected to react with oxygen and produce oxides, accompanied by luminescence. The number of free radicals was seen by them to increase with applied voltage [10-12].

As displayed in figure 7(f), the conversion time of the epoxide rings to acid molecules (t_c) varies from 666 h to 5.96 min for dielectric side-walls. The conversion time for dielectric side-walls is comparatively much higher than for dielectric anode. Conversion of all epoxide rings to acid molecules would cause an increase in surface conductivity of side-walls of narrow channel. It is reasonable to suppose that increased surface conductivity would lead to easy movement of charged particles along the side walls and consequently a situation where no voltage can effectively be supported along the length of narrow channel; this might cause PD extinction. Dissado et al. [22, 37] reported that movement of charges on the narrow channel wall can led to short-circuit a discharge.

In this work, we see that the time required for conversion of dielectric side-walls to conductive walls, is two times greater in magnitude orders than the time needed for the dielectric anode. This indicates that it might be expected that after a sufficient number of spark-type pulses, there would be a change in the nature of the discharge i. e. from pulse-type to glow. It is therefore unlikely that the discharge along a narrow channel would be extinguished with time; rather a transition in the nature of the discharge is likely to occur. This corroborates the results by Hudon et al who reported the occurrence of glow discharges at very long times [1, 2].

The effect of applied electric field on the magnitude of trapped charge on the dielectric side-walls of the narrow channel during one PD pulse is depicted in figure 7(g). A larger number of charges (mostly electrons) reaches the dielectric side-walls at higher fields. Auckland et al [48, 49] confirmed that avalanches within the gas-filled channel generate charges which are deposited on the walls or are trapped within the solid, reducing the voltage across the channel and extinguishing further avalanches. The initial luminosity of the breakdown originates within the solid, before a visible discharge occurs in the gas. Finally, increase in applied electric field will increase ionization and the number of impacts per discharge and, as a result will tend to cause greater cumulative damage over time as well as increase in surface conductivity.. At higher fields, the increased degradation is due to an increase in the number of impacting charged particles, in spite of decrease in average impact energy. The required time to convert narrow channel side-walls to a conductive surface (t_c) is much longer in compare with the required time for dielectric anode, and this is true for all values of electric field. This means that the transition from spark to glow discharges occurs at smaller time-scales than discharge extinction at all values of electric field. While increased number of impacts is accompanied by a decrease in the average energy at the impact site, the amount of charge deposited to surrounding dielectrics increases.

4.2. Micro-Channel Length

In this section, the effect of channel length on the extent of damage is considered. The electron group composition for different channel lengths (not shown here), indicates that for larger narrow channel-lengths (L_x), the total number of electrons increases significantly. As an electron traverses larger distances to reach the cathode (applied electric field remaining the same), greater amount of ionization occurs. Results obtained by Serra et al [19] similarly show that the number of electrons generated inside the cavity increases with cavity length. A comparison of the EEDFs for various lengths shown in figure 8(a) indicates that the proportion of cold electrons increases with length, and the average kinetic energy of the electrons at the dielectric anode decreases (figure 8(c));

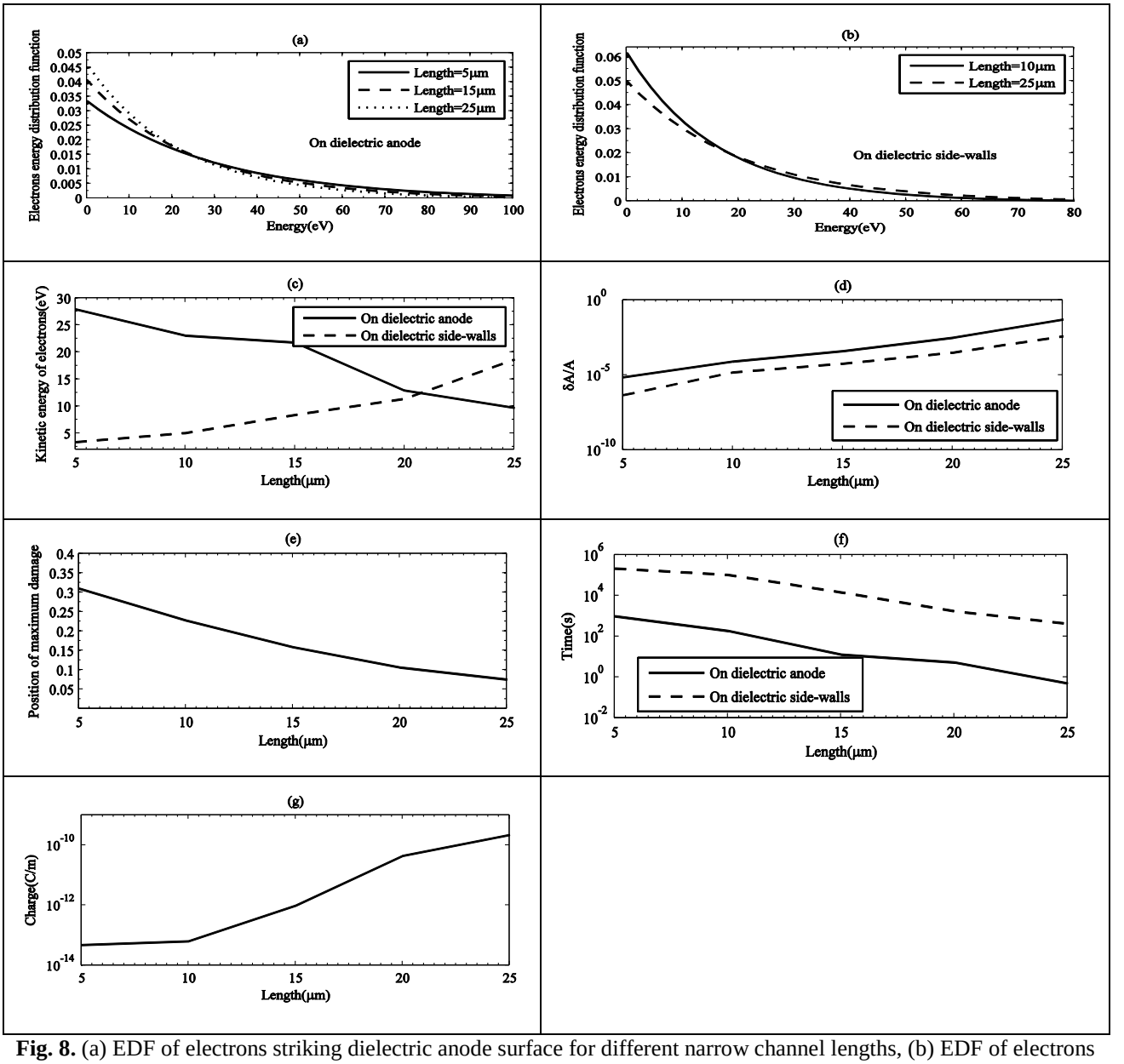

Fig. 8. (a) EDF of electrons striking dielectric anode surface for different narrow channel lengths, (b) EDF of electrons striking dielectric side walls, (c) Average kinetic energy of electrons at dielectric anode and side wall as a function narrow channel length, (d) Variation of fractional area damaged (δA/A) during one PD pulse on dielectric anode and side-walls as a function of narrow channel length, (e) Distance (normalized) from anode of region of maximum damage (x^D/L_x) on dielectric side walls, (f) The time of conversion of entire of epoxide rings to acid molecules (t_c) On dielectric anode and side-walls versus narrow channel length, (g) Charge trapped to narrow channel side-walls during one single PD pulse versus narrow channel length

i.e. increase in the number of charged particles results in larger number of collisions, but also reduced mean free path. Thus, lower energies are gained by the moving electrons during transition, and greater losses incurred with increased collisions. Interestingly, the probability of electrons belonging to the middle energy groups (20 eV-50 eV) does not change significantly for the lengths considered. The increase in degradation of the dielectric anode as seen in figure 8(d) is therefore, primarily due to the increase in the total number of electrons with sufficient energies. As seen in figure 8(e), the region of maximum damage on the dielectric side walls (x^D/L_x) appears closer to the anode as micro-channel length increases.

It is also observed that he damage on dielectric side-walls increases with narrow channel length. But, contrary to the situation at the dielectric anode, increase in length causes a larger percentage of hotter electrons to impact the dielectric side walls (figure 8(b)). Consequently, in figure 8(c), the average kinetic energy at the dielectric side-walls increases with increase in length. A simple parametric fit on fractional damaged area (δA/A) for dielectric anode and side walls, indicates an almost equivalent proportionality of damage at dielectric anode and side-walls with channel length (figure 8(d)):

$$\begin{matrix} \left(\frac{\delta A}{A}\right)_{\text{anode}} \propto (L_x)^{13.8} \\ \left(\frac{\delta A}{A}\right)_{\text{side-wall}} \propto (L_x)^{13.14} \end{matrix} . \quad (17)$$

With narrow channel length, the rate of conversion of epoxide rings to acid molecules (t_c) increases and conversion time (t_c) decreases (figure 8(f)). The values of t_c for the dielectric anode vary from 16.9 min for a 5 μm narrow channel length to 0.512 s for a 25 μm. On the other hand, it is perceived in figure 8(f) that **t**he conversion time (t_c) for dielectric side-walls vary from 60.55 h for 5 μm to 7.2 min for 25 μm. Interestingly, t_c for both dielectric anode and side walls decreases with narrow channel lengths. This means that PD pulses in long narrow channels are more likely to be extinguished due to voltage collapse across the narrow channel. In figure 8(g), the number of charges trapped on the side-walls is observed to increase significantly with channel length. Wu et al. [50] showed that as length of narrow channel increases, the effect of the field due to charged particles inside the narrow channel becomes more evident.

Thus, we conclude that greater cumulative damage with time and increase in surface conductivity occurs at higher narrow channel lengths. The two orders of difference in the values of the conversion time of epoxide rings to acid molecules (t_c) for dielectric anode and side-walls is true for all values of narrow channel length. Thus increase in channel length is likely to cause transition from spark to glow discharges before the cessation of discharge.

4.3. Micro-Channel Width

In this section, simulations are performed for the operating parameters presented in the table 2, except for the width which is varied between 1 to 100 μm.

Energy composition groups of electrons which are impacting dielectric anode and side-walls (not shown here) indicate that for greater channel widths (L_y), the total number of electrons decreases. By increasing the narrow channel width, there is a greater likelihood of movement of charge carriers and collisions in a direction perpendicular to the applied electric field (y-direction). Therefore, ionization and production of new charged particles reduces. Gu et al varied the channel diameter in the range of 50 to 600 μm [51], and found that the ionization coefficient increases rapidly as channel diameter decreases. This is in agreement with our results.

A comparison of the EEDFs for various narrow channel widths in figure 9(a) shows that the proportion of colder electrons increases at smaller widths. This results in a lower average kinetic energy for the narrower channels as seen in figure 9(c). This means less damage at the dielectric anode for wider narrow channels, as seen in figure 9(d). Figure 9(e) shows that the region of maximum damage on the dielectric side-walls moves closer to the anode as width decreases. As it is shown in figure 9(d), the damage on dielectric side-walls decreases with width. The EEDFs on dielectric side-walls for various narrow channel widths is plotted in figure 9(b). Decreased damage is a consequence of decreased number of electron impacts, which lowers the average kinetic energy. However, it may be noted that a difference in narrow channel width by two orders of magnitude has a very moderate effect on the extent of damage. Montanari et al. have also shown that the damage growth rate in PE is higher for cavities with smaller radii [21, 22].

As displayed in figure 9(f), the width of narrow channel has the same effect on required time to convert all epoxide rings to acid molecules (t_c) on both the dielectric anode and side-walls. Due to larger number of electrons reaching the dielectric anode and side-walls at lower widths, increase in surface conductivity is higher at lower channel widths. The time of conversion of epoxide rings to acid molecules (t_c) for dielectric anode varies from 5.38 s for a width of 1 μm to 36.33 min for a width of 100 μm. For dielectric side-walls, the variation in t_c is 27.2 min for a width of 1 μm to 5.33 h for a width of 100 μm. This means that PD is more likely to be extinguished due to voltage collapse

along the length of narrow channel, when the channel is narrower.

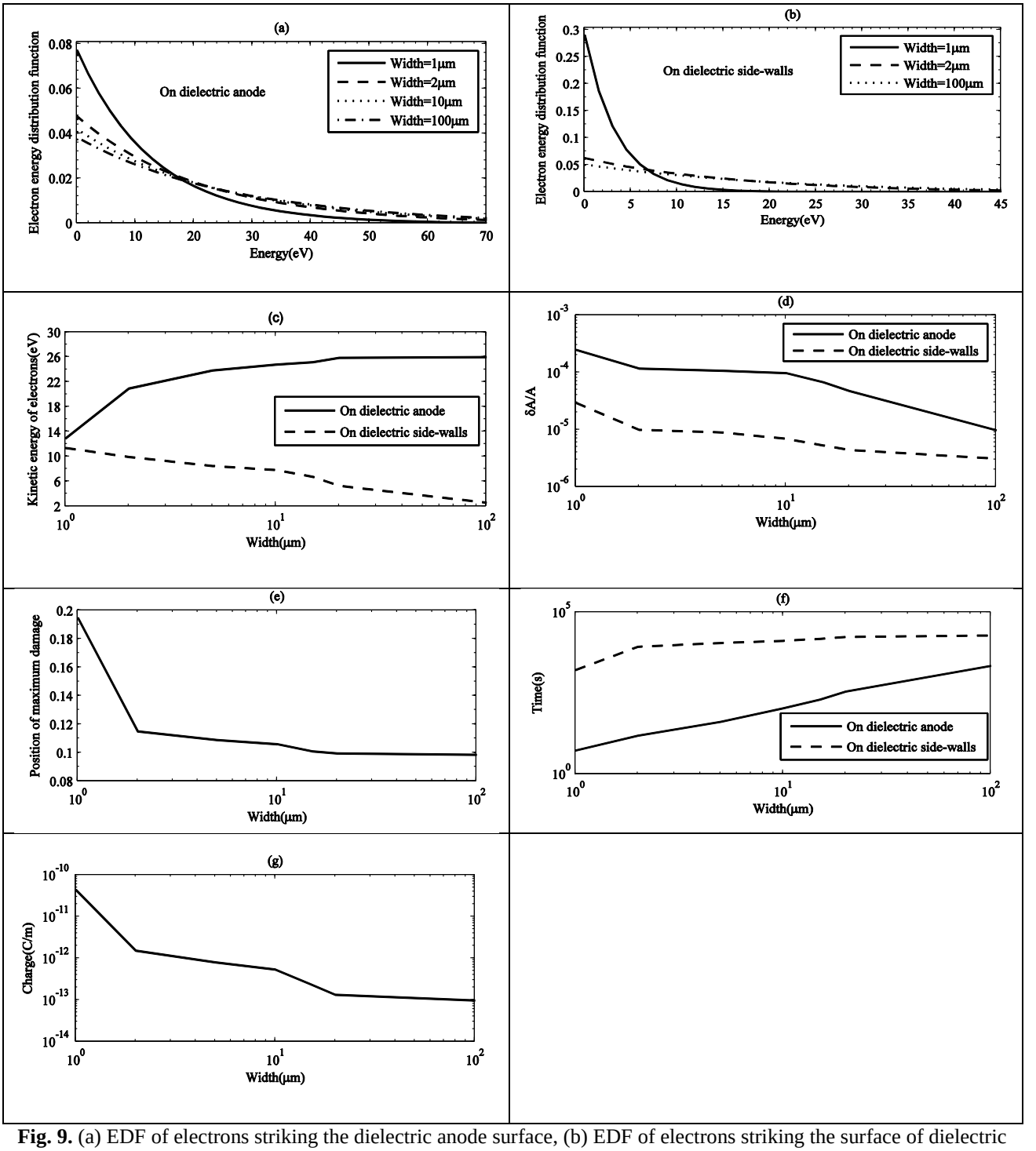

Fig. 9. (a) EDF of electrons striking the dielectric anode surface, (b) EDF of electrons striking the surface of dielectric side walls, (c) Average kinetic energy of electrons striking the dielectric anode and side walls, (d) Variation of fractional area damaged (δA/A) during one PD pulse on dielectric anode and side-walls as a function of electric field across narrow channel, (e) Distance (normalized) from dielectric anode of region of maximum damage (x^D/L_x) on dielectric side walls, (f) The time of conversion of entire of epoxide rings to acid molecules (t_c) On dielectric anode and side-walls as a function of narrow channel width, (g) Charge trapped to narrow channel side-walls during one single PD pulse as a function of narrow channel width

As a consequence of decreased number of electron impacts at the side-walls of wider narrow channels, as shown in figure 9(g), the amount of charged deposited on the side-walls reduces. Auckland et al. [48, 49] studied the influence of diameter on the quantity of charge trapped on the side-walls of a micro-channel in specimens with diameters in the range 50 to 126 μm and length of 10 mm. While the model of discharge propagation in their experiments is different (streamer as opposed to pulses), he observed a reduction in the amount of trapped charges with diameter of channel.
According to Wu et al. [50], in wider narrow channels, charges are less likely to be trapped on the channel-walls; for they quickly move to the channel end before the next PD pulse. Morshuis [52] showed that voids with small diameters (l-4 mm) showed similar discharge mechanisms as voids with width of 40 mm. Our findings also show that the effect of width on discharge is low especially when compared with other parameters such as applied electric field, narrow channel length, etc. In fact, increase in the width of narrow channel decreases the extent of degradation and that is due to decrease in the number of impacting charged particles.

4.4. Gas Pressure within micro-channel

In this section, the effect of gas pressure within the narrow channel is studied. Gas pressure plays an important role in ionization process in small cavities [53-55]. The effective ionization coefficient is a property of the gas and is therefore affected by the changing gas chemistry and by a change of pressure in the cavity.
Simulations are performed for the operating parameters presented in the table 2. Figure 10(a) and 10(b) show the effect of pressure (P_g) on the electron energy distribution at the dielectric anode and side-walls. Pressure increasing will develop the proportion of cold electrons both at the dielectric anode and side-walls. Lower pressures encourage larger mean free paths as electrons are accelerated by the applied field along the channel. At higher pressures, frequent collisions cause considerable energy loss, resulting in reduced average electron temperature at the dielectric anode. This is also borne out by a decrease in average kinetic energy shown in figure 10(c). Interestingly, the average kinetic energy saturates beyond a certain pressure level (approximately 800 Torr).
Figure 10(d) shows the extent of damage measured as the fractional area of damage, δA/A, during one PD pulse as a function of gas pressure. Despite an increased percentage of cold electrons and lower average kinetic energy, the cumulative effect of degradation by a larger number of charged particles evidently causes increased degradation at higher pressures. A similar effect is seen on the dielectric side-walls. A parametric fit on the fractional damaged area (δA/A) (figure 10(d)), indicates a somewhat higher rate of increase in damage at the dielectric anode, compared to the dielectric side-walls:

$$\begin{matrix} \left(\frac{\delta A}{A}\right)_{\text{anode}} \propto (P_g)^{4.45} \\ \left(\frac{\delta A}{A}\right)_{side-wall} \propto (P_g)^{3.97} \end{matrix} , \quad (18)$$

where $(\delta A/A)_{\text{anode}}$ and $(\delta A/A)_{\text{side-walls}}$ are the fractional damaged areas on dielectric anode and side-walls. As it is shown in figure 10(e), the region of maximum damage occurs nearer the anode at higher pressures. This corroborates the observations by Wu et al. that the damage by PD becomes more concentrated near the needle tip as gas pressure is raised [56].
As shown in figure 10(f), notwithstanding the increase in the number of low energy electrons and lower average kinetic energy, the cumulative effect of production of epoxide radicals by a larger number of charged particles causes time of conversion of all epoxide groups to acid molecules (t_c) to decrease at higher pressures. The time varies from 31.4 s for a pressure of 76 Torr to 4.3 s for a pressure of 1260 Torr for dielectric anode. It shows that the variations in (t_c) with pressure is comparatively lower than other parameters described in this work. The effect of pressure on t_c of the dielectric side-walls is similar to that on the dielectric anode. The values of t_c for side-walls varies from 44.44 h for a pressure of 76 Torr to 8 min for a pressure of 1260 Torr. Thus an increase in gas pressure inside the narrow channel might cause a transition from spark-type to glow discharge, but the discharge is more likely to extinguish due to increased surface conductivity of dielectric side-walls. Dissado et al. stated that increase in gas pressure is often observed to be associated with the cessation of tree discharges [22, 37].

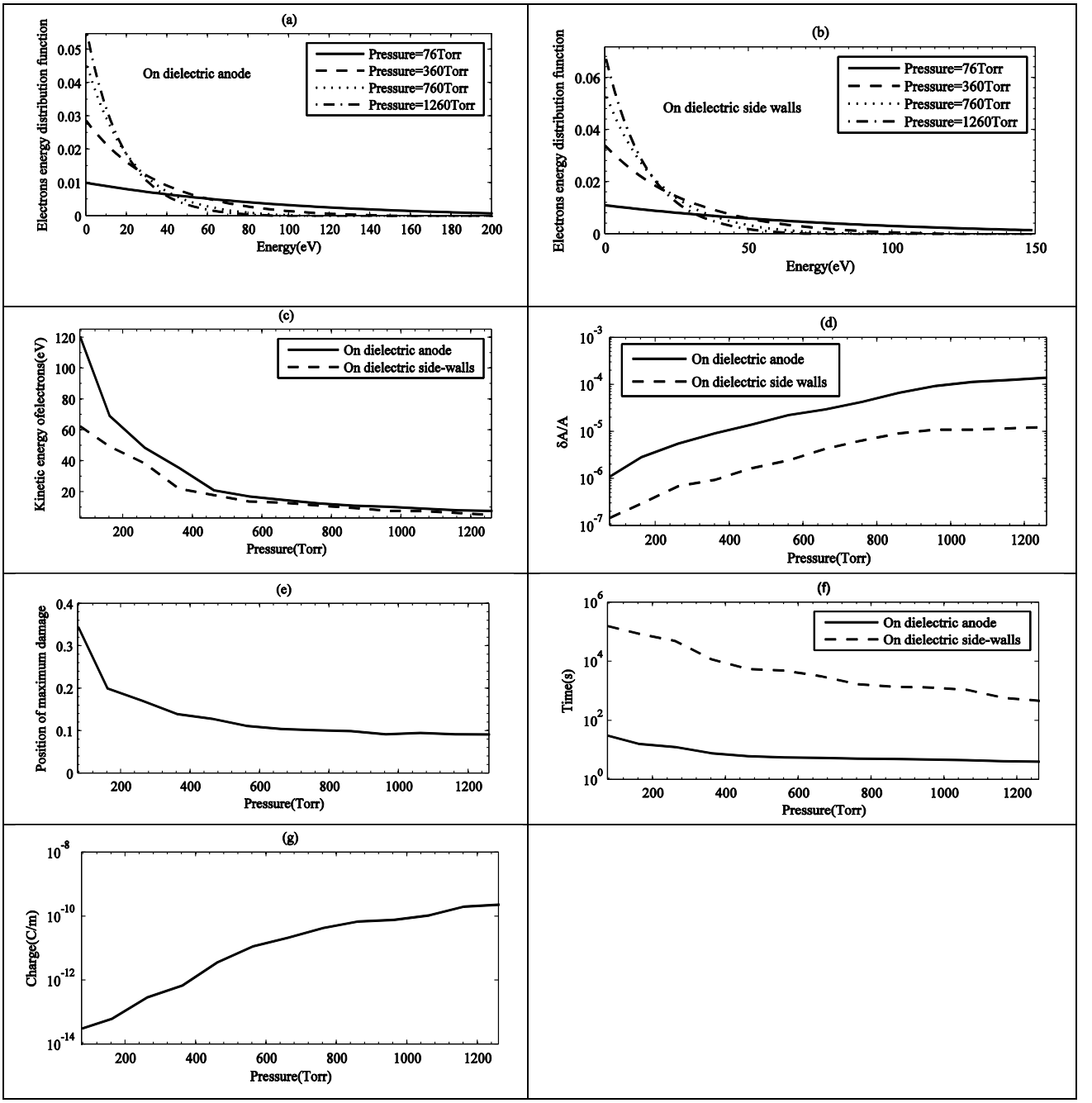

Fig. 10. (a) EDF of electrons at anode for different values of gas pressure inside narrow channel, (b) EDF of electrons at dielectric side walls, (c) Average kinetic energy of electrons at dielectric anode and side walls as a function gas pressure, (d) Variation of fractional area damaged (δA/A) during one PD pulse on dielectric anode and side-walls as a function of gas pressure during one PD pulse, (e) Distance (normalized) from anode of region of maximum damage (x^D/L_x) on dielectric side walls, (f) The time of conversion of entire of epoxide rings to acid molecules (t_c) On dielectric anode and side-walls as a function of gas pressure inside the narrow channel, (g) Charge trapped to narrow channel side-walls during one single PD pulse as a function of gas pressure inside narrow channel

The effect of gas pressure on the magnitude of charge trapped on the dielectric side-walls of the narrow channel during one PD pulse is depicted in figure 10(g). Owing to higher ionization at higher pressures, a larger number of charged particles (mostly electrons) will reach the dielectric side-walls at higher pressures. Briefly, at higher gas pressures, greater cumulative damage over time and consequently increase occurs in surface conductivity. The two orders of difference in

the magnitude of t_c for dielectric anode and side-walls is true for all values of gas pressure within narrow channel and is likely to cause transition in the nature of PD from spark to glow discharges rather than cessation of discharge.

5. CONCLUSIONS

The 2D kinetic model is used to perform a parametric analysis of degradation at the end of the narrow dielectric channel, as well as on the surroundings dielectrics of walls. The dependence of surface conductivity and damage progress on various physical parameters as well as stress variables is obtained.

Summarily, it is observed that the extent of damage caused by a PD, is primarily determined by the total number of impacting electrons capable of producing bond-scission at the dielectric anode. An increase in the number of energetic electrons at the dielectric anode increases effective damage as well as surface conductivity of surrounding dielectrics (as with increase in field).

It is clear from the parametric study undertaken in this paper that the two most important factors affecting extent of damage and increase in surface conductivity are the length of the narrow channel and the applied electric field. Increase in length causes an increase in the total number of electrons reaching the dielectric anode, due to increased ionization as well as high energies gained from acceleration in the field. High electric fields have a similar effect, due to the production of a large quantity of high energy electrons. High background gas pressure tends to decrease the mean free path and average energy gained by the electrons from the electric field, and thus the increase in degradation is moderated. That is to say that, operating conditions which increase ionization are tend to cause greater cumulative damage over time and consequently increase in surface conductivity. In situations where increased number of impacts is accompanied by a decrease in the average energy at the impact site, the extent of degradation is a trade-off between the number of particles, and the decrease in average impact energy.

It is shown that the time required to convert all the epoxide rings to acid molecules (t_c) on both dielectric anode and side-walls decreases as electric field, length of narrow channel, gas pressure increase while this time increases with channel width.

It is also seen that there is considerable damage on the dielectric side-walls, but the region of damage is concentrated near to the anode (0.1-0.3 of the total length).

An important point to be noted is that the damage caused by a single pulse in terms of C-H bond scissions is very low, and significant damage would only be produced by consistent and repeated PD pulses over a long period of time. This is in agreement with the fact that damage due to PD pulses is a slow ageing process, and does not lead to direct an immediate failure. Degradation of the dielectric anode at the end of the narrow channel would result, over time, in elongation of the channel (narrow channel progression). Transition of narrow channel growth to catastrophic failure takes place due to the synergy between various breakdown mechanisms (thermal, mechanical and chemical), and even an extension by a few micro-meters may have catastrophic effect. The estimation of damage therefore is expected to be useful in developing a life-model with firmer grounding on the actual physical processes involved.

Also, the conversion of a conductive pit due to graphitization of the polymer by carbon formation, ahead of the channel would strongly affect local field intensification. Apart from bond-scission, electrons impacting the polymer might cause several kinds of anion production, and over repeated pulses, considerable space charge trapping would occur at the end of the channel. It has been shown that space charge at the narrow channel tips, and in the volume of the dielectric ahead of a narrow channel, plays a significant role in the nature of narrow channel growth [24].

Space charge accumulation on the channel walls would significantly affect the discharge in the channel. Also, bond-scission would result in increased conductivity of the channel walls through formation of acid molecules. These may cause cessation of PD pulse as well as shield the channel from the external field, possibly even leading to PD suppression [25, 26].

Thus in this paper, the fundamental nature of energetic electron interactions with dielectrics surrounding narrow channels are studied. The EDF's related to positive ions on the cathode dielectrics and negative ions on the anode dielectric are also presented. Though, they are found to be irrelevant from the point of view of scission.

6. APPENDIX

The total charge density σ_T on the anode metallic electrode may be expressed by [25]:

$$\sigma_T^t = \sum_{j=0}^{N-1} \sigma_{0j}^t \qquad \text{(A1)}$$

where σ_{0j}^t is the surface charge density on anode electrode at time '*t*'. The simplified form of equation (26) of [25] for a 'simple metallic-metallic' configuration (ref. [24]) is:

$$\sigma_T^t = \frac{\varepsilon_0}{\Delta x} N\phi_0^t - \frac{\varepsilon_0}{\Delta x} \sum_{j=0}^{N-1} \phi_{1j}^t - \frac{\Delta x}{2} \sum_{j=0}^{N-1} \rho_{0j} \qquad \text{(A2)}$$

where, ϕ_0^t, ϕ_{1j}^t, N are the potential on the anode at '*t'*, potential at $x_1(=1\times\Delta x)$ and number of divisions along y-axis. Particle '*p'* contributes to Q_{ij} through the space charge density ρ_{ij} (bilinear weighting: [25]).

The equivalent circuit for the narrow channel bounded by dielectrics is shown in figure 2(b). C_g, C_d and C_r represent the equivalent capacitances of the gap, the dielectric layers and dielectric material parallel to the micro-channel respectively, and J_{conv} is the discharge current density. The time variation of σ_T, the total charge density on the driven dielectric electrode, may be obtained from the Kirchhoff 's Current Law:

$$A\frac{d\sigma_s}{dt} = I_{ext} - I_r + AJ_{conv} \tag{A4}$$

where I_{ext}, σ_T and I_r the total external current, charge on the dielectric surfaces and current in the dielectric material parallel to the narrow channel.

The time variation of voltage drop (U_d) across the dielectric slab is obtained as:

$$C_d\frac{dU_d}{dt} = I_{ext} - I_r \cdot \tag{A5}$$

Figure 2(b) shows a simple external circuit consisting of a voltage source in series with a capacitor coupled to the left electrode. The voltage drop V_c across the capacitor in the external circuit is obtained from voltage balance as,

$$V_c = V(t) - 2U_d - \phi_0 \tag{A6}$$

V(t) is the applied voltage source. The discrete finite differenced form of (A4) can be expressed as:

$$A(\sigma_T^t - \sigma_T^{t-1}) = Q_c^t - Q_c^{t-1} - Q_r^t + Q_r^{t-1} + Q_{conv}^t \tag{A7}$$

where $\int Idt = Q_c = CV_c$ and $\int I_r dt = Q_r = CU_r$ are the charge on the external capacitor and bulk of dielectric material parallel to the narrow channel, and Q_{conv}^t is the charge deposited on the electrode from the discharge in the cavity during the time interval (t-1, t). Combining equations (A6) and (A7) we obtain:

$$\sigma_T^t = \sigma_T^{t-1} + \frac{1}{A}(CV(t) - (C+C_r)\varphi_0^t - 2(C+C_r)U_d^t + Q_r^{t-1} - Q_c^{t-1} + Q_{conv}^t) \tag{A8}$$

Similarly, the discrete finite differenced form of (A5) can be expressed as:

$$U_d^t - U_d^{t-1} = \frac{1}{C_d}\int (I_{ext} - I_r)dt = \frac{Q_c^t - Q_c^{t-1} - Q_r^t + Q_r^{t-1}}{C_d} \tag{A9}$$

If we combine equations (A6) and (A9), then we have:

$$U_d^t = \frac{U_d^{t-1} + \frac{1}{C_d}(CV(t) - (C+C_r)\varphi_0^t - Q_c^{t-1} + Q_r^{t-1})}{1 + (C+C_r)/C_d} \tag{A10}$$

By inserting the value of U_d^t to the equation (A8) and taking $\alpha=(1+2(C+C_r)/C_d)^{-1}$, the value of σ_T^t can be written as follow:

$$\sigma_T^t = \sigma_T^{t-1} + \frac{1}{A}(\alpha CV(t) - \alpha(C+C_r)\varphi_0^t - 2\alpha(C+C_r)U_d^{t-1} - \cdot \alpha Q_c^{t-1} + \alpha Q_r^{t-1} + Q_{conv}^t) \tag{A11}$$

Equations (A1), (A2) for σ_T^t and (A11) can be combined and solved for ϕ_0^t on dielectric anode to produce:

$$\varphi_0^t = (\sigma_{s_T}^{t-1} + \frac{1}{A}(\alpha CV(t) - \alpha Q_c^{t-1} + \alpha Q_r^{t-1} - 2\alpha(C+C_r)U_d^{t-1} + Q_{Conv}^t) + \frac{\Delta x}{2}\sum_{j=0}^{j=N}\rho_{0j} + \frac{\varepsilon}{\Delta x}\sum_{j=0}^{j=N}\varphi_{1j}^t)(\frac{\varepsilon}{\Delta x}N + \alpha(C+C_r)/A)^{-1} \tag{A12}$$

7. ACKNOWLEDGMENT

I would like to appreciate the Institute of Science and High Technology and Environmental Sciences for financial support within the project 1.140-90/2/24.

REFERENCES

[1] C., Hudon, R., Bartnikas, **"Surface conductivity and gas phase reactions arising with epoxy exposed to partial discharges"**, *IEEE CEIDP*, pp. 725-34, 1992.

[2] C., Hudon, R., Bartnikas and M.R., Wertheimer, **"Spark-to-glow discharge transition due to increased surface conductivity on epoxy resin specimens"**, *IEEE TDEI*, Vol.28, No.1, pp. 1-8, 1993.

[3] C., Hudon, R., Bartnikas and M.R., Wertheimer, **"Effect of 64hysic-chemical degradation of epoxy resin on partial discharge behavio**r", *IEEE TDEI*, Vol.2, No.6, pp. 1083-1094, 1995.

[4] C., Hudon, R., Bartnikas and M.R., Wertheimer, **"Surface conductivity of epoxy specimens subjected to partial discharges"**, *IEEE International Symposium on Electrical Insulation, Toronto, Canada*, pp. 3-6, 1990.

[5] C., Hudon, R., Bartnikas and M.R., Wertheimer, **"Chemical and physical degradation effects on epoxy surfaces exposed to partial discharges"**, *4th International Conference on Properties and Applications of Dielectric Materials, Brisbane Australia*, pp. 811-814, 1994.

[6] P.H.F., Morshuis , F.H., Kreuger, **"Transition from streamer to Townsend mechanisms in dielectric voids"**, *J. Phys. D: Appl. Phys.*, Vol.23, pp. 1562-1568, 1990.

[7] T., Ishida, Y., Mizuno, M., Nagao and M., Kosaki, **"Computer aided partial discharge analyzing system for detection of swarming pulsive microdischarges"**, *IEE Conference Publication*, No. 378, pp. 99-100, 1993.

[8] C., Mayoux, G., Garcia and J., Sarlaboux**, "Interaction of corona with dielectric material until damage"**, *IEEE TEI*, Vol. EI-17, No.2, pp. 156-162, 1982.

[9] E.J., McMahon, J.R., Perkins**, "Surface and volume phenomena in dielectric breakdown of polyethylene"**, *IEEE TPAS*, Vol.82, No.69, pp. 1128-1136, 1963.

[10] D., Briggs, C.R., Kendall, A.R., Blythe and A.B., Wootton, **"Electrical discharge treatment of polypropylene film"**, *Polymer*, Vol. 24, pp. 47-52, 1983.

[11] D., Briggs , C.R., Kendall, **"Derivation of discharge-treated LDPE: an extension of XPS analysis and a probe of specific interactions in adhesion"**, *Int. J. Adhesion and Adhesive*, pp. 13-17, 1982.

[12] D., Briggs, D.G., Rance, C.R., Kendall and A.R., Blythe, **"Surface modification of poly (ethylene terephthalate) by electrical discharge treatment"**, *Polymer*, Vol. 21, pp. 895-900, 1980.

[13] D., Briggs , C.R., Kendall**, "Chemical basis of adhesion to electrical discharge treated polyethylene",** *Polymer*, Vol. 20, pp.1053-1054, 1979.

[14] A.R., Blythe, D., Briggs, C.R., Kendall, D.G., Rance and V.J.I., Ziehy, **"Surface modification of polyethylene by electrical discharge treatment and the mechanism of autoadhesion"**, *Polymer*, Vol. 19, pp. 1273-1278, 1978.

[15] M., Gamez-Garcia, R., Bartnikas and M.R., Wertheimer, **"Synthesis reactions involving XLPE subjected to partial discharges"**, *IEEE TEI*, Vol.EI-22, No.2, pp. 199-205, 1987.

[16] E.C., Rogers, E.B., Grad, and V.G., Harriss, **"A servo-mechanism for the study of self-extinction of gaseous discharges in cavities in dielectrics"**, *J. Sci. Instrum*., Vol.33, pp. 7-10, 1956.

[17] T., Tanaka, Y., Ikeda, **"Internal discharges in polyethylene with an artificial cavity"**, *IEEE TPAS*, Vol. PAS-90, No. 6, pp. 2692-2702, 1971.

[18] D.W., Auckland, S.M.F., Kabir and B.R., Varlow, **"Charge deposition in gas filled channels with insulating walls",** *IEE proceedings-A*, Vol.140, No.6, pp. 509-516, 1993.

[19] S., Serra, G.C., Montanari, and Mazzanti, **"Theory of inception mechanism and growth of defect-induced damage in polyethylene cable insulation"**, *J. Appl. Phys*., Vol.98, pp. 034102-1-15, 2005.

[20] G., Mazzanti, G.C., Montanari and F., Civenni, **"Model of inception and growth of damage from microvoids in polyethylene-based materials for HVDC cables part 1: theoretical approach"**, *IEEE TDEI*, Vol.14, No.5, pp. 1242-1254, 2007.

[21] G., Mazzanti, G.C., Montanari and F., Civenni**, "Model of inception and growth of damage from microvoids in polyethylene-based materials for HVDC cables part 2: parametric investigation and data fitting"**, *IEEE TDEI*, Vol.14, No.5, pp. 1255-1263, 2007.

[22] L.A., Dissado, G., Mazzanti and G.C., Montanari, **"Propagation of electrical tree structures in solid polymeric insulation"**, *IEEE TDEI*, Vol.4, No.5, pp. 496-596, 1997.

[23] J.P., Novak , R., Bartnikas, **"Ionization and excitation behavior in a micro-cavity"**, *TDEI*, Vol.2, No.5, pp. 724-728, 1995.

[24] A.A., Ganjovi, N., Gupta and G.R.G., Raju, **"A kinetic model of a PD pulse within voids of sub-millimeter dimensions",** *IEEE TDEI*, Vol.16, No.6, pp. 1743-1754, 2009.

[25] V., Vahedi , G., DiPeso, **"Simultaneous Potential and Circuit Solution for Two-Dimensional Bounded Plasma Simulation Codes",** *J. Comput. Phys*., Vol.131, pp. 149-163, 1997.

[26] V., Vahedi, , C.K., Birdsall, M.A., Lieberman, G., DiPeso, and T.D., Rognlien, **"Verification of frequency scaling laws for capacitive radio-frequency discharges using two-dimensional simulations"**, *Phys. Fluids B*, Vol.5, pp. 2719-2729, 1993.

[27] W., S. Lawson, **"Particle simulation of bounded 1D plasma systems"**, *J. Comput. Phys*., Vol.80, pp. 253-276, 1989.

[28] G.G., Raju, **"Gaseous Electronics: Theory and Practice, Boca Raton"**,. *FL: Taylor and Francis*, 2005.

[29] C.K., Birdsall, **"Particle-in-cell charged-particle simulations, plus Monte Carlo collisions with neutral atoms, PIC–MCC***"*, *IEEE Trans. Plasma Sci*., Vol.19, pp. 65–85, 1995.

[30] V., Vahedi, , M., Surendra**, "Monte-Carlo collision model for particle-in-cell method: application to argon and oxygen discharges"**, *Comput. Phys. Commun*., Vol.87, pp. 179–98, 1995.

[31] C., K. Birdsall , A.B., Langdon, **"Plasma physics via computer simulation"**, *McGraw-Hill, New York*, 1985.

[32] A., Roldan, J., M. Perez, A., Williart, F., Blanco, and G., Garcia, **"Energy deposition model for low-energy electrons (10-10 000 eV) in air"**, *J. Appl. Phys.*, Vol.95, No.10, pp. 5865-5870, 2004.

[33] W., Zhang, T.S., Fisher, and S.V., Garimella, **"Simulation of ion generation and breakdown in atmospheric air"**, *J. Appl. Phys*., Vol.96, pp. 6066-6072, 2004.

[34] P.J., Mardahl, , K.L., Cartwright, **"Reducing numerical heating in 1-D PIC simulations",** *Annual Progress Report for 1993, Plasma Theory and Simulation Group, University of California Technical Memorandum, Electronics Research Laboratory*, Berkeley, 1993.

[35] P.J., Mardahl , J.P., Verboncoeur, **"Charge conservation in electromagnetic PIC codes; spectral comparison of Boris/DADI and Langdon-Marder methods**", *Comp. Phys. Comm*., Vol.106, pp. 219-229, 1997.

[36] J.P., Verboncoeur, **"Symmetric spline weighting for charge and current density in particle simulation"**, *Journal of Comput. Phys*., Vol.174, pp. 421-427, 1997.

[37] L.A., Dissado, G., Mazzanti, G.C., Montanari**, "The role of trapped space charges in the electrical aging of insulating materials"**, *IEEE TDEI*, Vol.4, No.5, pp. 496-596, 1997.

[38] S., Prasad, T., Grover and S., Basu, **"Coarse-Grained molecular dynamics simulation of cross-linking of DGEBA epoxy resin and estimation of the adhesive strength"**, unpublished.

[39] N., Shimizu, C., Laurent, **"Electrical tree initiation"**, *IEEE TDEI*, Vol. 5, No. 5, pp. 651-659, 1998.

[40] K.D., Wolter, J., Tanaka, and J.F., Johnson, **"A study of the gaseous degradation products of corona-exposed polyethylene"**, *IEEE TET*, Vol. E1-17, No.3, pp. 248-252, 1982.

[41] P.H.F., Morshuis , F.H., Kreuger, **"The spatial distribution and electrical parameters of partial discharges in polyethylene insulation during aging"**, *Proc. 4th Int. Conf. Cond. Breakd. Solid Diel., Sestri Levante/Italy*, pp. 209-214, 1992.

[42] R., Bartnikas, **"Some observations on the character of corona discharges in short gap spaces",** *IEEE TEI*, Vol.6, No. 2, pp. 63-75, 1971.

[43] R., Bartnikas**, "Engineering Dielectrics",** *Vol. I, Corona Measurement and Interpretation, SlT669, ASTM*, Philadelphia, 1979.

[44] R. Bartnikas**, "Discharge rate and energy loss in helium at low frequencies"**, *Electrical Engineering*, Vol. 52, pp. 348-359, 1969.

[45] R. Bartnikas, "Note on ac discharges between metallic-dielectric electrodes in helium", *J. Appl. Phys*., Vol. 40, pp. 1974-1976, 1969.

[46] J.P., Novak, R., Bartnikas, **"Quantitative model of a short-gap breakdown in air"**, *XVIIth International symposium on discharge and electrical insulation in vacuum, Berkeley*, pp. 60-64, U.S., 1996.

[47] K., Kaminaga, T., Suzuki, T., Uozumi, T., Haga, N., Yasuda and T., Fukui, **"The mechanism of degradation of polyethylene in a high electrical field",** *Conference on Electrical Insulation and Dielectric Phenomena*, pp. 666-71, 1993.

[48] D.W., Auckland, A.B., Borishade, and R., Cooper, **"The breakdown characteristics of air-filled tubules in solid insulation"**. *IEEE Conference Publication* No. 129, *Dielectric Materials, Measurements and Applications, Cambridge* pp. 15-18, July 1975.

[49] D.W., Auckland, A.B., Borishade, and R., Cooper, **"Photographic investigation of breakdown of composite insulation"**. *Proc. IEE*, Vol.124, No.12, pp. 1263-1266, 1977.

[50] K., Wu, Y., Suzuoki, T., Mizutani and H., Xie, **"Model for partial discharges associated with treeing breakdown: I. PDs in tree channels"**, *J. Phys. D: Appl. Phys*., Vol. 33, pp.1197–1201, 2000.

[51] W.Y., Gu, C., Laurent, and C., Mayoux, **"Characteristics of discharges inside simulated tree micro-cavities under impulse voltage"**, *J. Phys. D: Appl. Phys*., Vol.19, pp. 2197-2207, 1986.

[52] P.H.F., Morshuis and F.H., Kreuger, **"Transition from streamer to Townsend mechanisms in dielectric voids"**, *J. Phys. D: Appl. Phys*., Vol. 23, pp. 1562-1568, 1990.

[53] P., Morshuis, **"Assessment of dielectric degradation by ultrawide-band PD detection"**, *IEEE TDEI*, Vol.2, No. 5, pp. 744-760, 1995.

[54] C., Mayoux , C., Laurent, **"Contribution of partial discharges to electrical breakdown of solid insulating materials"**, *IEEE TDEI*, Vol.2, No.4, pp. 641-652, 1995.

[55] R.J., Densley, **"An investigation into the growth of electrical trees in XLPE cable insulation"**, *IEEE TEI*, Vol. EI-14, No.3, 1979.

[56] K., Wu, Y., Suzuoki, T., Mizutani and H., Xie, **"Model for partial discharges associated with treeing breakdown: II. Tree growth affected by PDs"**, *J. Phys. D: Appl. Phys*., Vol.33, pp.1202–1208, 2000.

[57] R.J., Densley, R., Bartnikas and B., Bernstien, **"Multiple stress aging of solid-dielectric extruded dry-cured insulation systems for power transmission cables",** *IEEE TPD*, Vol.9, No.1, pp. 559-571, 1994.

[58] H.J., Wintle**, "Schottky injection currents in insulators: the effect of space charge on the time dependence"**, *IEEE TEI*, Vol. 12, No. 6, pp. 424-428, 1977.